Bright matter-wave solitons: summary of experimental techniques

L. Khaykovich[1]

Department of Physics, Bar Ilan University, Ramat-Gan, 52900 Israel.
hykovl@mail.biu.ac.il

1 Introduction

A uniform 3D BEC with attractive interactions is unstable because the gas tends to infinitely increase its density in order to decrease its interaction energy. This limitation is remarkably removed by an external trapping potential which stabilizes the system by introducing zero-point kinetic energy [1, 2]. For an attractive BEC in a trap there is thus a critical number of atoms N_c below which the condensate is stable. Increasing number of atoms in the BEC leads to the collapse of the gas just as in the uniform case. First experiments with attractively interacting trapped Bose gases were carried out with lithium atoms in their doubly polarized state (in which the nuclear and electronic spin components have the largest possible values along the direction of the magnetic field) [3]. Later the experiments with ^{85}Rb (using tunable interactions) explored quantitatively the dependence of the critical number of atoms N_c on the strength of interatomic interactions [4]. The dynamics of growth and collapse of BECs with attractive interactions has been directly investigated in two notable experiments with ^{7}Li [5] and ^{85}Rb [6].

Remarkably, the 3D collapse can be readily avoided if a BEC is confined in only two directions. Along the free direction, the condensate dispersion owing to its kinetic energy is balanced by the attractive interatomic interactions, resulting in the formation of bright solitons[1]. These solitons were demonstrated in two independent experiments with ^{7}Li atoms [7, 8]. The similar approaches used in both experiments, demonstrate the spectacular flexibility of recently developed experimental techniques for manipulating ultracold dilute atomic gases. In this chapter we shall discuss these techniques starting with tunable interatomic interactions achieved by means of Feshbach resonances. We then describe the optical trapping of atomic BECs and the reduction to low dimensional (1D and 2D) condensates. Next, we discuss the experimental demonstrations of solitons in Paris [7], Rice [8] and the more recent demonstration of solitons with ^{85}Rb atoms in a nearly 3D trap

[1] Strictly speaking, they are solitary waves rather than solitons as their collisions are inelastic (see Sec. 5). However we shall refer to them as solitons throughout this chapter.

in Colorado [9]. Finally we discuss the prospects of bright soliton collisions experiments and the origin of higher order nonlinearity which is expected to appear in them.

2 Tunable interatomic interactions

2.1 Feshbach resonance

Collisions in ultracold gases are extensively discussed in lectures [10] and books [1, 2]. Here we shall only emphasize a few crucial points, while for full details we refer the reader to the literature.

Alkali atoms which are widely used in BEC experiments have a single electron outside closed shells. If we neglect for the following the magnetic dipole-dipole interactions (which introduce inelastic dipolar loss mechanism) the scattering potential of a pair of atoms is a central potential $V(r)$, where r is the atomic separation. The long-range part of the potential is due to van der Waals electric dipole-dipole attraction and it's strongest contribution is of the form $-1/r^6$ while the short-range potential is dominated by strong repulsion due the overlap of electron clouds. Generally the interaction potential $V(r)$ can be decomposed to singlet $V_S(r)$ and triplet $V_T(r)$ terms depending on the spin state of the two electrons:

$$V(r) = V_S(r)P_S + V_T(r)P_T \tag{1}$$

where P_S and P_T are projection operators to singlet and triplet spin states. The singlet potential is in general much deeper than the triplet one because two electrons can occupy the same orbital (valence electron attraction).

The well established result of the scattering theory for the van der Waals type potential (decreasing sufficiently fast at infinity) is that the low energy scattering is isotropic ($s-wave$ scattering) and characterized by a single parameter a called the scattering length [11]. Potentials for most alkali atoms are generally very well known thanks to their intensive study in cold atoms experiments. Scattering lengths for lithium isotopes have been measured by photoassociative spectroscopy and found to be (for bosonic ^7Li) $a_S = 1.7\pm0.1$ nm (singlet) and $a_T = -1.46\pm0.03$ nm (triplet) [12]. Scattering lengths of ^{85}Rb were determined to be $a_S = 127^{+32}_{-18}$ nm and $a_T = -19.5\pm0.8$ nm in a Feshbach resonance study [13]. Scattering lengths for other alkali atoms are available in literature [1].

The scattering length defines all essential properties of the BEC and, most excitingly, it is variable and can be altered by either a shape resonance [10] or, now widely and successfully used in experiments, a Feshbach resonance. This most powerful experimental technique allows tuning of strength and sign of interatomic interactions by simple change of an external magnetic field. Ever since their first experimental observation [14], Feshbach resonances revolutionized the field of cold atoms research, providing the experimentalists with unprecedented level of control. We shall therefore briefly discuss the origin of the resonance. For extensive discussion we refer the reader to review papers on the subject [15].

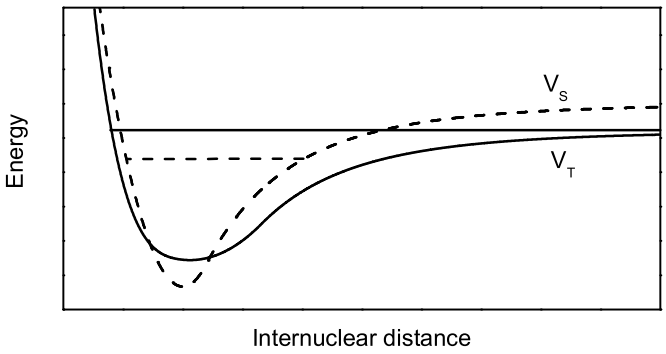

Fig. 1. Schematic representation of singlet and triplet interatomic potentials. Solid line shows the triplet interaction potential which is the entering channel of two colliding atoms. It can be shifted by means of a magnetic field offset to meet a bound state of the singlet potential (dashed line). The latter is the interaction potential of two atoms when the hyperfine interaction flips the spin of one of them. Feshbach resonance takes place when two energies (a triplet continuum and a singlet bound state) coincide.

Two-atom scattering Hamiltonians can be represented most generally by two single atom Hamiltonians and the interaction potential $V(r)$. The single atom Hamiltonian includes hyperfine interaction term of the form $V_{HF} = \mathcal{E}_{HF}\mathbf{S}_i\mathbf{I}_i$ where $\mathbf{S}_i$ is the electronic and $\mathbf{I}_i$ is the nuclear spin. However the interatomic potential (Eq. (1)) depends on the *total* electronic spin $\mathbf{S}^2 = (\mathbf{S}_1 + \mathbf{S}_2)^2$ which does not commute with the hyperfine interaction term. In a collision process the hyperfine term can flip electronic spins and introduce coupling between the interaction potentials. Consider two atoms with their electronic spins $m_1 = m_2 = -1/2$ in a magnetic field B so that they are polarized and interact through a triplet potential. The continuum of the triplet potential lies below the continuum of the singlet potential because the latter one belongs to a different energy level which approaches a higher energy hyperfine state at low magnetic field. The resonance occurs when there is a bound state in the singlet potential which is close to the continuum of the triplet potential (see Fig. 1). Most significantly the resonance condition can be reached by simple change of the external magnetic field as only atoms interacting through a triplet potential are affected. Near the Feshbach resonance the scattering length a is predicted to vary dispersively as a function of the magnetic filed B [15]:

$$a(B) = \tilde{a}\left(1 - \frac{\triangle}{(B - B_0)}\right) \tag{2}$$

where $\tilde{a}$ is the off-resonance background scattering length and $\triangle$ represents the width of the resonance.

In Fig. 2 the variation of effective scattering length with magnetic field around a Feshbach resonance, is shown for ^7Li atoms in their absolute ground state. Divergence around the magnetic field of 725 G is the signature of the resonance. Excluding the resonance there is an evolution of scattering potential from a com-

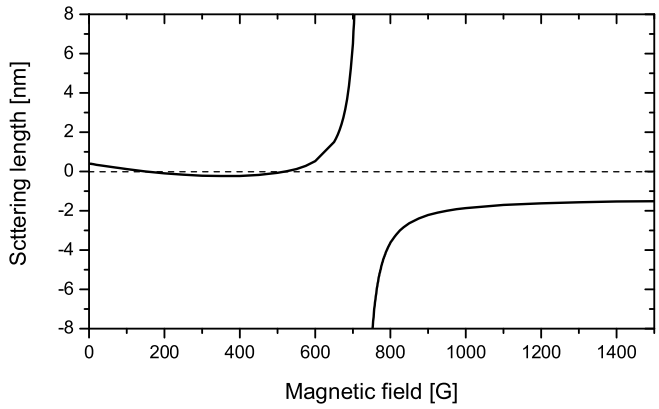

Fig. 2. Calculated magnetic field dependence of the scattering length for ^7Li in the absolute ground state [7]. The resonance position is at 725 G.

bination of triplet and singlet potentials at zero magnetic field (with the scattering length $a = 0.4$ nm) to the purely triplet one (with the scattering length $a_T = -1.46$ nm) at high magnetic field. Combination of the two effects provides a very wide range of magnetic fields where the scattering length is negative and very small which suits perfectly the requirement for soliton production.

There is however, an inherent obstacle in the use of Feshabach resonances because they affect both elastic and *inelastic* collision rates. Consequently, severe limitations are set on the practical increase of the scattering length. This apparent drawback was put to good use in experiments, allowing for the accurate location of the resonance. Strong loss of atoms associated with different inelastic processes provides a simple and reliable experimental signature of the Feshabch resonance[2] [14]. In Fig. 3 inelastic scattering loss is shown for the theoretically predicted resonance of Fig. 2.

Applications of the Feshbach resonance are very diverse. Here we discuss only one of them which is the observation of matter-wave solitons. Other applications include the study of BCS transition, BEC-BCS crossover and molecular BEC in a two-spin-mixture fermi gas [17], coherent atom-molecule oscillations with bosons [18] and many others that constantly emerge.

2.2 Measure of the interaction strength

An insight into the behavior of a BEC with attractive interactions can be obtained by means of a variational approach (see previous contribution and books [1, 2]). The collapse is predicted to occur when

$$k_c = \frac{N_c|a|}{a_{ho}} \approx 0.67 \tag{3}$$

[2] Fermionic atoms constitute a remarkable exception to this rule, in that they are extremely stable against inelastic losses in the vicinity of a Feshabch resonance [16].

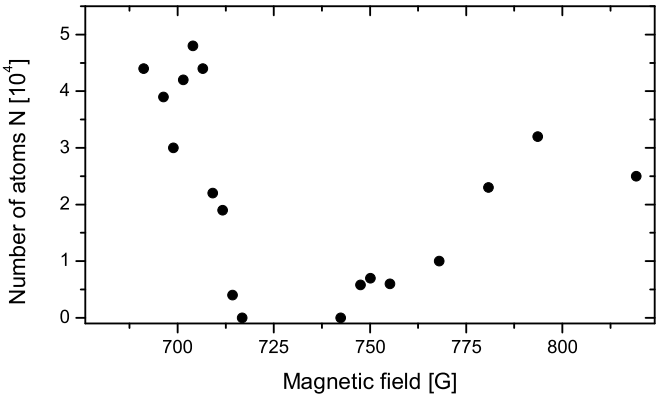

Fig. 3. Observation of a ^7Li Feshbach resonance through a rapid loss associated with the three-body recombination (two-body relaxation is impossible from the absolute ground state).

where $a_{ho} = \sqrt{\hbar/m\omega_{ho}}$ is the mean harmonic oscillator length and N_c is the critical number of atoms. Experimentally somewhat lower value of $k_c = 0.46 \pm 0.06$ has been found [13].

The dimensionless parameter $k = N|a|/a_{ho}$ is very useful as a measure of interaction strength. For repulsive condensates ($a > 0$) in 3D trap the usual situation is $k >> 1$. In this strongly interacting (Thomas-Fermi) limit, the kinetic energy of the condensate can be neglected and the Gross-Pitaevskii equation (GPE) is approximately solved by the familiar parabolic density profiles [1, 2]. For attractive condensates ($a < 0$) the k parameter should always be less than k_c according to Eq. (3). In a cylindrically symmetric trap which tightly confines atoms in two spatial dimensions, an accurate approximation of the 1D gas can be made when the interaction energy is small with respect to the radial potential energy level spacing. The GPE then reduces to an effective 1D form:

$$i\hbar\psi_t = -\frac{\hbar^2}{2m}\psi_{xx} + g_{1D}|\psi|^2\psi + \hbar\omega_r\psi, \tag{4}$$

where $g_{1D} = 2a\hbar\omega_r$ is the renormalized quasi-1D interaction constant [19] and ω_r is the oscillation frequency in radial direction. The condensate wavefunction is well described by a Gaussian in the radial direction and a well known functional form of a bright soliton in the longitudinal (unbound) direction:

$$\psi(x,t) = e^{-i\mu t/\hbar}\frac{1}{\sqrt{2l}}\frac{1}{\cosh(x/l)}, \tag{5}$$

where l is the spatial extent of the soliton and $\mu = -\hbar^2/2ml^2$ is the chemical potential. Substituting Eq. 5 into Eq. 4 yields

$$l = \frac{2\hbar^2}{g_{1D}Nm} = a_r \frac{a_r}{N|a|} = \frac{a_r}{k_r}, \tag{6}$$

where $a_r = \sqrt{\hbar/m\omega_r}$ is the radial harmonic oscillator length and $k_r = N|a|/a_r$ is the 'radial' interaction strength.

In the 1D limit ($k_r << 1$) the longitudinal size of the soliton exceeds significantly its radial size. If however the interaction parameter k_r increases, the condensate wavepacket shrinks in mainly longitudinal direction, approaches its 3D limit and, ultimately, collapses. $k_r << 1$ requires small atom number and/or weak interactions (small scattering length). Tuning of the scattering length to low values via the Feshbach resonance allows one to weaken interactions and thus to increase the number of atoms and to improve signal/noise ratios.

3 Optical confinement of Bose-Einstein condensates

3.1 BEC in optical traps

The possibility to tune interactions usually requires optical trapping as Feshbach resonance frequently occurs in states that cannot be magnetically trapped. Optical traps which rely on electric dipole interaction of an atom with far-detuned light offer the possibility to trap atoms in all internal states [20]. The optical potential imposed on an atom by a far-detuned laser is given by

$$U(\mathbf{r}) = \frac{\hbar\gamma^2}{8I_s}\frac{I(\mathbf{r})}{\delta}, \tag{7}$$

where δ is the laser detuning from the atomic resonance, I_s is the saturation intensity (which is usually of the order of a few mW/cm^2) and γ is the natural linewidth of the excited state of atom. It is immediately seen from Eq. (7) that the red (blue) detuned laser provides attractive (repulsive) potential. The attractive potential is most simply formed by focusing a single infrared laser beam into the center of the atomic cloud. This method is now widely used in many ultracold atom experiments [20].

Apart from the conservative potential $U(\mathbf{r})$, the laser light induces heating on atoms through spontaneous scattering of photons and power and position instabilities. To reduce heating by spontaneous emission very far detuned lasers are used (as the scattering rate scales as I/δ^2). In experiments [7, 8] infrared (1.06μm) Nd:YAG lasers were used that provided almost 400 nm detuning from the atomic resonance (for Li atoms). Power and position jitters can be also, if necessary, controlled by the active feedback stabilization methods.

Initial pursuit of BECs by all-optical techniques was unsuccessful, though it stimulated development of numerous beautiful experimental techniques such as sub-recoil optical cooling [21], various optical dipole and lattice traps [20] and optical molasses [22], Raman sideband [23] and evaporative cooling [24] in such traps. The winning strategy for BEC however was proved to be the evaporative cooling in a magnetic trap. After being produced in the magnetic trap, the BEC

was then transferred into an optical trap and various effects have been studied including the first experimental demonstration of a Feshbach resonance in sodium BEC [14].

Continued efforts toward 'all-optical' BECs were finally rewarded with ^{87}Rb [25] and ^{133}Cs [26] condensates obtained directly in optical traps. In the case of ^{87}Rb this method increased significantly the rate of BEC production as optical confinement can be easily made much stronger than that of a magnetic trap. The resulting condensates were F=1 spinors [25]. However the main driving force beyond the search for all-optical ways to reach BEC threshold, was failed attempts to observe BEC of Cs atoms in a magnetic trap. Strongly enhanced two-body losses from the magnetically trappable states has blocked the 'standard' way to a Cs BEC [27].

Within the context of optical trapping, one should also mention the very intensive use of periodic optical potentials, having an immense impact on many cold-atom activities including solitons (see contribution to this volume on Optical lattice potentials and Gap solitons).

3.2 BEC in low dimensions

Optical traps allow extreme control over trapping potentials and provide highly anisotropic configurations where the motion of atoms can be extinguished in one or two directions. This modifies significantly the behavior of the system for both attractive and repulsive condensates. In the attractive case highly anisotropic quasi-1D potential are essential to make 1D bright (and dark) solitons as was discussed in Sec. 2.2. For repulsive condensates consequences of the reduced dimensionality are very rich.

The 1D limit is obtained when the interaction energy becomes smaller than the energy level spacing of the external potential in tightly bound radial direction. In this regime the size of the condensate wavefunction in the radial direction only slightly deviates from the Gaussian size of the ground state. This was experimentally observed by measuring the condensate released energy in both lithium [28] and sodium condensates [29]. Very elongated quasi-1D trapping geometries causes condensate fragmentation or, in other words, realization of quasi-condensates which locally behave like ordinary condensates but do not possess a globally uniform phase [30]. In these limits the collisional properties of atoms remain essentially 3D and the GPE stays relevant. At very low densities and very strong radial confinement a different limit of 1D systems, called Tonks-Girardeau gas of "impenetrable bosons", has been recently experimentally observed [31]. This achievement provides now a new playground for the exciting subject of strongly correlated 1D quantum systems.

The 2D limit can be obtained in a pancake type trapping geometry with the tight confinement in only one direction. Experimentally it is achieved by either using cylindrical optics or retro-reflecting laser beam to build a standing wave which provides an array of pancake traps. The regime where interaction energy was smaller than the energy level spacing in the trap was experimentally shown

in ref [29]. The most significant challenge for 2D systems however is the observation of different types of a phase transition associated with the emergence of a topological order providing binding of vortex-antivortex pairs. This Berezinskii-Kosterlitz-Thouless (BKT) phase transition occurs at finite temperature and was very recently observed in a stack of optical pancake traps [32].

4 The experiments

4.1 Formation of a single soliton

An experiment in Paris which demonstrated formation of a single soliton, used lithium atoms in their absolute ground state trapped in a far detuned 1D optical dipole trap (a waveguide) [7]. We briefly discuss the apparatus and experimental procedure here while for full details we refer the reader to the original paper. Atoms from a thermal lithium beam are slowed in a Zeeman slower and loaded into a magneto-optical trap. These atoms are then transferred by means of a magnetic elevator into a Ioffe-Pritchard-type magnetic trap in a doubly polarized spin state $F = 2, m_F = 2$. In this state the scattering length is negative, relatively large ($a = -1.4$ nm) and insensitive to the external magnetic field. Evaporatively precooled to about 10 μK, atoms are then loaded into a far detuned optical dipole trap formed by the intersection of two Nd:YAG laser beams oriented vertically and horizontally. Optically trapped atoms are then transferred to the lowest energy state ($F = 1, m_F = 1$) to take advantage of the magnetic tuning of the scattering length via a Feshbach resonance. The following evaporation step is performed at the magnetic field of 665 G where $a = 2.1$ nm (see Fig. 2) by lowering the depth of the optical potential. A condensate with $N \approx 2 \times 10^4$ atoms is formed in a nearly isotropic trap. The scattering length is then tuned to zero to reduce three-body losses and the trap is adiabatically deformed into a cylindrically symmetric trap. The effective interaction is then tuned to the attractive regime by lowering the magnetic field strength to 425 G where $a = -0.21$ nm and the vertical laser beam is switched off completely by a mechanical shutter releasing the atomic cloud in an effective 1D optical waveguide (a horizontally oriented laser beam potential). At variable delays after switching off the vertical laser beam, the atomic cloud is measured by the absorption imaging technique.

The time evolution of an ideal gas ($a = 0$ at $B = 520$ G) in a waveguide is compared with a gas with attractive interactions ($a = -0.21$ nm at $B = 425$ G) in Fig. 4. In the propagation direction the current coils that are used to provide an offset magnetic field produce a slightly expulsive potential which overcomes the dipole trap. When the vertical laser beam is switched off, the atomic cloud is projected on the slop of this potential because of a small offset between the atomic initial position and the maximum of the potential. This causes a unidirectional drift toward the left (see Fig. 4). The width of the expanding cloud in the waveguide is considerably broader in the noninteracting case while for all observation times

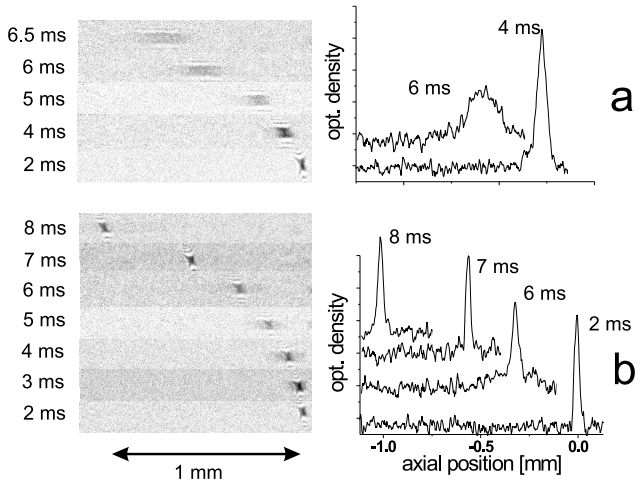

Fig. 4. Propagation of an ideal BEC (a) and of a soliton (b) in the horizontal 1D waveguide in the presence of an expulsive potential. Corresponding profiles in the propagation direction are integrated over the vertical direction (reprinted from [7]).

the soliton's width remains equal to the resolution limit of the imaging system[3]. The soliton is observed to propagate over a macroscopic distance of 1.1 mm in 10 ms without decay.

Stability analysis which is done numerically by variational techniques shows a very narrow parameter region where the soliton could survive between the 3D collapse and the explosion imposed by the external expulsive potential [7]. For the radial harmonic oscillator length $a_r = 1.4\mu$m and $a = -1.4$nm, the number of atoms that allows the soliton to be formed is $4.2 \times 10^3 \leq N \leq 5.2 \times 10^3$. Clearly, the expulsive potential imposes severe limitation on soliton research and should be avoided. In a later theoretical paper however, an interesting phenomenon of soliton destabilization by quantum evaporation which can occur in a repulsive potential has been proposed [34].

4.2 Soliton trains

In another experiment at Rice, formation and propagation of matter-wave soliton trains are observed rather than a single soliton [8]. Small differences in the experimental realization with that, discussed in the previous section lead to different results. The stages until loading into an optical trap are essentially the same. The main difference however is in the realization of an optical trap. In the Rice experiment the optical trap consists of a focused infrared Nd:YAG laser for radial

[3] More recently it was shown numerically that the soliton under the expulsive potential is not truly invariant in size [33]

confinement and two cylindrically focused doubled Nd:YAG beams (blue-detuned repulsive optical potential) 250 μm apart, providing end-caps for longitudinal confinement. The evaporative cooling is then performed in this trap when the uniform magnetic field is ramped to a value of 700G ($a = 10.6$ nm) until the threshold to a BEC. Then the magnetic field is reduced to a value of 575G where a is small and negative.

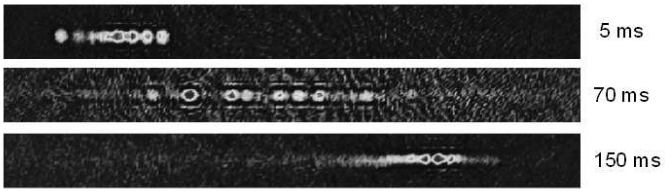

Fig. 5. Soliton train oscillation in the longitudinal potential. The solitons group at the turning points and spread out in the middle of the oscillation (reprinted by permission from Macmillan Publishers Ltd: [8], copyright (2002)).

Soliton behavior is investigated by setting them in motion. This is achieved by displacing the infrared laser focus axially from the center of the magnetic trap and the end-caps. In this way the BEC is initially formed on the side of the weak longitudinal potential of the infrared laser beam and was held there by the green laser end-caps. On removing the end-caps, the atoms oscillate in the longitudinal potential for a varying duration before being imaged (Fig. 5). As can be seen in images, a solitons train was created rather than a single soliton. Moreover the solitons bunch at the turning points and spread out in the middle. The immediate conclusion is that there are repulsive interactions between neighboring solitons although the interatomic interactions are attractive.

It is a very well known that two neighboring solitons with π phase difference interact repulsively. In Fig. 6 the relative spacing between solitons in the trap as a function of propagation time is shown. An explanation of the formation of soliton trains was suggested by the presence of the alternating phase structure. When the scattering length is changed from positive to negative the condensate becomes unstable to the growth of perturbations at a particular wavelength. The available length scale in a BEC is a healing length $\xi = 1/8\pi n|a|$ where n is the atomic density. In the repulsive condensate the phase is constant, but as the sign of the scattering length is switched, a mode with wavelength ξ becomes unstable so that initial quantum fluctuations imprint the condensate with an alternating phase structure [35]. Although simplified, the numerical simulations were able to produce up to seven solitons with alternating phases. The model suggested that the number of solitons produced should vary with the initial size of the condensate which was verified in the experiment.

The mechanism responsible for the formation of the soliton train and the long-term stability of solitons are as yet not completely understood. Another model

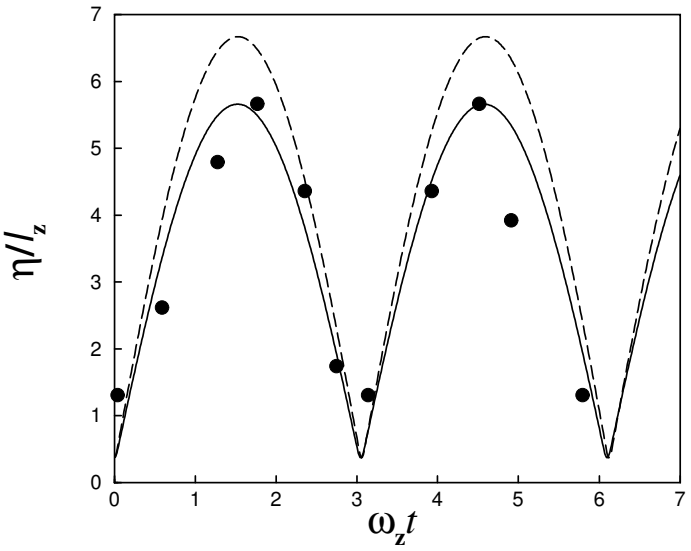

Fig. 6. Relative spacing between two neighboring solitons in the trap. The vertical axis is soliton separation in units of longitudinal harmonic oscillator length. The solid curve is a solution of the equation of motion of two solitons and the dashed curve neglects the interatomic attraction in the soliton interaction potential. The points are experimental data (reprinted with permission from [35], copyright (2002) by the American Physical Society).

suggests that self-interference fringes seed the perturbation modes and that the solitons within a train are actually created with arbitrary phases [36]. After a series of collapses induced by collisions between attracting solitons, a final stable configuration is achieved in which only repelling solitons remain. It was experimentally observed that the total number of atoms in the train was about a fifth of the initial atom number in the repulsive condensate. Another model [37] also suggests that solitons are formed with arbitrary phases and the following time evolution shows missing peaks in soliton trains which can be identified in the experimental data of ref [8].

4.3 Formation of solitons in nearly 3D trap

In a different experiment with ^{85}Rb atoms, a robust configuration of multiple solitons was created in a nearly symmetric magnetic trap during the collapse of an attractive condensate [9]. This experiment starts with the production of a stable condensate within the positive scattering length region of a broad Feshabch resonance which exists on a magnetically trappable state $|F = 2, m_F = -2>$ at the field $B = 155$G [38]. The radial (longitudinal) frequency of cylindrically symmetric trap was 17.3 Hz (6.8 Hz) where condensates of up to 1.5×10^4 atoms were formed. The collapse of the condensate was then induced by quickly switching

the scattering length through zero to a variable negative scattering lengths. The number of atoms surviving the collapse was then investigated as a function of a final negative scattering length. Most remarkably the number of atoms in the remnant attractive condensates was significantly greater than the critical number (for example at $a = -5.3$ nm the remnant condensate contained about 10 times more atoms than the critical value). This curious discrepancy was interpreted as a formation of multiple solitons which were identified on absorption images as distinct clouds (see Fig. 7). The solitons oscillate for over three seconds colliding more than 40 times during this period. The remarkable stability of the soliton dynamics in the 3D trap was considered as a manifestation of π phase shift between the neighboring solitons. This conclusion was supported by numerical simulations of the experiment based on 3D GPE [39]. However the origin of the alternating π phase shifts rest unresolved.

5 Origin of higher order nonlinearity and its impact on soliton dynamics

In Sec. 2.2 bright soliton is introduced as a special solution of 1D GPE (Eq. (4)) and it is therefore a 1D object. However in all experiments discussed in Sec. 4 despite the differences in realizations of each specific trap where solitons were formed, the solitons themselves were similar in a sense of being almost 3D objects. In particular, in the Paris experiment [7], a stable soliton was only possible if its longitudinal size exceeded the transverse size by no more than 20%. In the experiment with *Rb* [9] the number of atoms per soliton was always close to N_c yielding solitons with almost complete spherical symmetry. It is an intuitive consequence of the soliton train formation process that solitons were formed containing of about the critical number of atoms and thus close to a 3D geometry. In Sec. 4.2 the mechanism responsible for the soliton train formation was identified as a modulation instability (MI) caused by the unstable phase modes with a wavelength ξ (the condensate healing length) which is (in 1D form):

$$\xi = \frac{a_r}{\sqrt{8n_{1D}|a|}}, \tag{8}$$

where $n_{1D} = n\pi a_r^2$ is the linear density. If the negative scattering length is small such that $k_r << 1$ (see Eq. 6), the denominator of Eq. (8) is very small yielding an effective 1D single soliton production (ξ is about the size of the initial condensate). However if $k_r > 1$, ξ becomes of the order of a_r very quickly. It can be seen by presenting the linear density as $n_{1D} = \lambda N/a_r$, where λ depends on the condensate longitudinal size before the scattering length is switched to a negative value. Assuming zero interactions for the initial conditions (as per ref. [7, 8]), $\lambda = a_r/a_l = \sqrt{\omega_l/\omega_r}$ where $a_l = \sqrt{\hbar/m\omega_l}$ is the longitudinal harmonic oscillator length. In the Paris experiment [7] $\lambda \approx 0.27$ yielding $\xi < a_r$ which leads to a collapse where most of atoms are lost and to a single soliton formation with almost 3D geometry. In the Rice and the later ^{85}Rb experiments [8, 9] the situations were

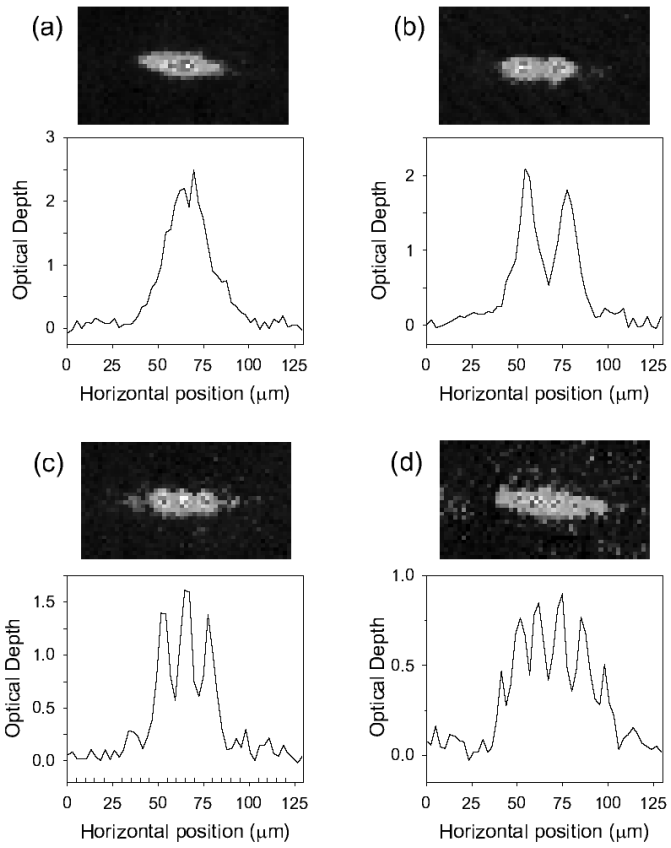

Fig. 7. Absorption images and cross sections of multiple solitons. When the negative scattering length a is small a single attractive condensate is formed with the number of atoms less than the critical number (a), for larger absolute value of the scattering length the condensate is split into a number of solitons (b)-(d) (reprinted with permission from [9], copyright (2006) by the American Physical Society).

very similar however soliton trains of nearly 3D solitons were observed rather than a single soliton. These differences can be explained by a presence of trapping rather than anti-trapping longitudinal potential and significantly bigger initial number of atoms.

Recently, it was shown that the proximity of the soliton to being a 3D object strongly affects its properties, such as the character of its motion [40], interactions [41] and collisions [42]. In particular, it is demonstrated that a moving soliton immersed in a cloud of thermal atoms is subjected to a temperature-dependent friction force [40]. In a different proposal, thermal environment causes the soliton to split into two partially coherent solitonic structures which are analogous to optical random-phase solitons [43]. A collision between two solitons, which are by themselves stable, in a confined geometry may readily lead to collapse, if the

total number of atoms in the soliton pair exceeds the critical value, and the phase difference between the solitons is (close to) zero [41]. A collision between two identical in-phase solitons can lead to a merger into a single pulse if their velocities are smaller than the critical velocity and symmetry breaking is readily obtained in collisions between two solitons with non-zero initial phase difference [42].

The way to avoid residual three-dimensionality in the experiments where multiple solitons are formed is to weaken the interaction strength after the formation process is completed. Experimental verification of different regimes and above theoretical proposals are still lacking.

6 Conclusions

Experimental observations of matter-wave solitons triggered vast theoretical research and many interesting questions have been raised. In this chapter we intended to show the state of the art experimental techniques that were recently developed in the field of ultracold atoms and allowed experimental demonstrations of different types of solitons. The power and flexibility of these techniques allow many intriguing tasks presented in theoretical proposals to become an experimental reality. More experimental techniques will be soon available as the interest in this research field grows fast.

7 Acknowledgments

I thank R.G. Hulet, H.T.C. Stoof and S.L. Cornish for providing me with the material from their original work. I am grateful to Amichay Vardi for a careful reading of the manuscript and suggesting various improvements. This work was supported, in a part, by the Israel Science Foundation.

References

1. C.J. Pethick, and H. Smith: *Bose-Einstein Condensation in Dilute Gases*, (Cambridge University Press, Cambridge 2002).
2. L. Pitaevskii, and S. Stringari: *Bose-Einstein Condensation*, (Clarendon Press, Oxford 2003).
3. C.C. Bradley, C.A. Sackett, J.J. Tollet, and R.G. Hulet, Phys. Rev. Lett. **75**, 1687 (1995); C.C. Bradley, C.A. Sackett, and R.G. Hulet, Phys. Rev. Lett. **78**, 985 (1997).
4. J.L. Roberts, N.R. Claussen, S.L. Cornish, E.A. Donley, E.A. Cornell, and C.E. Wieman, Phys. Rev. Lett. **86**, 4211 (2001).
5. G.M. Gerton, D. Strekalov, I. Prodan and R.G. Hulet, Nature **408**, 692 (2000).
6. E.A. Donley, N.R. Claussen, S.L. Cornish, J.L. Roberts, E.A. Cornell, and C.E. Wieman, Nature **412**, 295 (2001).
7. L. Khaykovich, F. Schreck, G. Ferrari, T. Bourdel, J. Cubizolles, L.D. Carr, Y. Castin, and C. Salomon, Science **256**, 1290 (2002).

8. K.E. Strecker, G.B. Partridge, A.G. Truscott and R.G. Hulet, Nature **417**, 150 (2002).
9. S.L. Cornish, S.T. Thompson, and C.E. Wieman, Phys. Rev. Lett. **96**, 170401 (2006).
10. J. Dalibard: Collisional dynamics of ultra-cold atomic gases. In: *Bose-Einstein Condensation in Atomic Gases*, Proceedings of the Enrico Fermi International School of Physics, vol CXL, ed by R. Inguscio, S. Stringari, and C.E. Wieman (IOS Press, Amsterdam 1999) pp 321–349;
11. L.D. Landau and E.M. Lifshitz: *Quantum Mechanics*, 3d edn (Pergamon Press, Oxford 1977), sect. 131.
12. E.R.I. Abraham, W.I. McAlexander, C.A. Sackett, and R.G. Hulet, Phys. Rev. Lett. **74**, 1315 (1995); E.R.I. Abraham, C.A. Sackett, and R.G. Hulet, Phys. Rev. A **55**, 3299 (1997).
13. J.L. Roberts, N.R. Claussen, J.P. Burke, C.H. Greene, E.A. Cornell, and C.E. Wieman, Phys. Rev. Lett. **81**, 5109 (1998).
14. S. Inouye, K.B. Davis, M.R. Andrews, J. Stenger, H.-J. Miesner, D.M. Stamper-Kurn, and W. Ketterle, Nature **392**, 151 (1998).
15. E. Timmermans, P. Tommasini, M. Hussein, and A. Kerman, Phys. Reports **315**, 199 (1999); R.A. Duine, and H.T.C. Stoof, Phys. Reports **396**, 115 (2004).
16. J. Cubizolles, T. Bourdel, S.J.J.M.F. Kokkelmans, G.V. Shlyapnikov, and C. Salomon, Phys. Rev. Lett. **91**, 240401 (2003).
17. M. Greiner, C.A. Regal, and D.S. Jin, Nature **426** 537 (2003); S. Jochim, M. Bartenstein, A. Altmeyer, G. Hendl, S. Riedl, C. Chin, J. Hecker Denschlag, and R. Grimm, Science **302**, 2101 (2003); M.W. Zwierlein, C.A. Stan, C.H. Schunck, S.M.F. Raupach, S. Gupta, Z. Hadzibabic, and W. Ketterle, Phys. Rev. Lett. **91**, 250401 (2003); T. Bourdel, L. Khaykovich, J. Cubizolles, J. Zhang, F. Chevy, M. Teichmann, L. Tarruell. S.J.J.M.F. Kokkelmans, and C. Salomon, Phys. Rev. Lett. **91**, 250401 (2003).
18. E.A. Donley, N.R. Claussen, S.T. Thompson, C.E. Wieman, Nature, **417**, 529 (2002).
19. Y. Castin: Bose-Einstein condensates in atomic gases: simple theoretical results. In: *Coherent Atomic Matter Waves* ed by R. Kaiser, C. Westbrook, and F. David (Springer, Berlin Heidelberg New York 2001) pp 1–136.
20. R. Grimm, M. Weidemüller, Y.B. Ovchinnikov, Adv. At. Mol. Opt. Phys. **42**, 95 (2000); N. Friedman, A. Kaplan and N. Davidson, Adv. At. Mol. Opt. Phys. **48**, 99 (2002).
21. F. Bardou, J.-P. Bouchaud, A. Aspect, and C. Cohen-Tannoudji: *Lévy Statistics and Laser Cooling*, (Cambridge University Press, Cambridge 2002).
22. S.L. Winoto, M.T. DePue, N.E. Bramall, and D.S. Weiss, Phys. Rev. A **59**, R19 (1999); M.T. DePue, C. McCormick, S.L. Winoto, S. Oliver, and D.S. Weiss, Phys. Rev. Lett. **82**, 2262 (1999).
23. S.E. Hamann, D.L. Haycock, G. Klose, P.H. Pax, I.H. Deutsch, and P.S. Jessen, Phys. Rev. Lett. **80**, 4149 (1998); H. Perrin, A. Kuhn, I. Bouchoule, and C. Salomon, Europhys. Lett. **42**, 395 (1998); V. Vuletić, C. Chin, A.J. Kerman, and S. Chu, Phys. Rev. Lett. **81** 5768 (1998); A.J. Kerman, V. Vuletić, C. Chin, and S. Chu, Phys. Rev. Lett. **84** 439 (2000).
24. C.S. Adams, H.J. Lee, N. Davidson, M. Kasevich, amd S. Chu, Phys. Rev. Lett. **74**, 3577 (1995).
25. M.D. Barrett, J.A. Sauer, M.S. Chapman, Phys. Rev. Lett. **87** 010404 (2001).
26. T. Weber, J. Herbig, M. Mark, H.-C. Nägerl, and R. Grimm, Science **299** 232 (2003).
27. J. Söding, D. Guéry-Odelin, P. Desbiolles, G. Ferrari, and J. Dalibard, Phys. Rev. Lett **80** 1869 (1998).

28. F. Schreck, L. Khaykovich, K.L. Corwin, G. Ferrari, T. Bourdel, J. Cubizolles, and C. Salomon, Phys. Rev. Lett. **87** 080403 (2001).
29. A. Görlitz, J.M. Vogels, A.E. Leanhardt, C. Raman, T.L. Gustavson, J.R. Abo-Shaeer, A.P. Chikkatur, S. Gupta, S. Inouye, T. Rosenband, and W. Ketterle, Phys. Rev. Lett. **87** 130402 (2001).
30. S. Dettmer, D. Hellweg, P. Ryytty, J.J. Arlt, W. Ertmer, K. Sengstock, D.S. Petrov, G.V. Shlyapnikov, H. Kreutzmann, L. Sanots, M. Lewenstein, Phys. Rev. Lett. **87**, 160406 (2001).
31. B. Paredes, A. Widera, V. Murg, O. Mandel, S. Fölling, I. Cirac, G.V. Shlyapnikov, T.W. Hänsch, I. Bloch, Nature **429**, 277 (2004); T. Kinoshita, T. Wenger, D.S. Weiss, Science **305**, 1125 (2004).
32. Z. Hadzibabic, P. Krüger, M. Cheneau, B. Battelier, and J. Dalibard, Nature **441**, 1118 (2006).
33. L. Salasnich, Phys. Rev. A **70**, 053617 (2004).
34. L.D. Carr and Y. Castin, Phys. Rev. A **66**, 063602 (2002).
35. U. Al Khawaja, H.T.C. Stoof, R.G. Hulet, K.E. Strecker, and G.B. Partridge, Phys. Rev. Lett. **89**, 200404 (2002).
36. L.D. Carr and J. Brand, Phys. Rev. Lett. **92**, 040401 (2004); L.D. Carr and J. Brand, Phys. Rev. A **70**, 033607 (2004).
37. L. Salasnich, A. Parola, L. Reatto, Phys. Rev. Lett. **91**, 080405 (2003).
38. S.L. Cornish, N.R. Claussen, J.L. Roberts, E.A. Cornell, and C.E. Wieman, Phys. Rev. Lett. **85**, 1795 (2000).
39. N.G. Parker, A.M. Martin, S.L. Cornish and C.S. Adams, cond-mat/0603059 (2006).
40. S. Sinha, A.Y. Cherny, D. Kovrizhin, and J. Brand, Phys. Rev. Lett. **96**, 030406 (2006).
41. B.B. Baizakov, B.A. Malomed and M. Salerno, Phys. Rev. A **70**, 053613 (2004), and an article in *Nonlinear Waves: Classical and Quantum Aspects*, ed. by F.Kh. Abdullaev and V.V. Konotop, pp. 61-80 (Kluwer Academic Publishers: Dordrecht, 2004).
42. L. Khaykovich and B.A. Malomed, Phys. Rev. A **74**, 023607 (2006).
43. H. Buljan, M. Segev, and A. Vardi, Phys. Rev. Lett. **95**, 180401 (2005).